

**NAVAL SURFACE WARFARE CENTER  
PANAMA CITY DIVISION  
PANAMA CITY, FL 32407-7001**



---

**TECHNICAL REPORT  
NSWC PCD TR-2017/006**

## **AUTOMATED THRESHOLD SELECTION FOR TEMPLATE-BASED SONAR TARGET DETECTION**

Frank J. Crosby  
Unmanned Systems, Automation & Processing Division (Code X20)  
Science & Technology Department

Bradley C. Marchand  
Applied Sensing and Processing Branch (Code X24)  
Unmanned Systems, Automation & Processing Division  
Science & Technology Department

**August 2017**

**DISTRIBUTION STATEMENT A:** Approved for public release: distribution unlimited.



<b>REPORT DOCUMENTATION PAGE</b>					<i>Form Approved OMB No. 0704-0188</i>	
<small>The public reporting burden for this collection of information is estimated to average 1 hour per response, including the time for reviewing instructions, searching existing data sources, gathering and maintaining the data needed, and completing and reviewing the collection of information. Send comments regarding this burden estimate or any other aspect of this collection of information, including suggestions for reducing the burden, to Department of Defense, Washington Headquarters Services, Directorate for Information Operations and Reports (0704-0188), 1215 Jefferson Davis Highway, Suite 1204, Arlington, VA 22202-4302. Respondents should be aware that notwithstanding any other provision of law, no person shall be subject to any penalty for failing to comply with a collection of information if it does not display a currently valid OMB control number.</small>						
<b>PLEASE DO NOT RETURN YOUR FORM TO THE ABOVE ADDRESS.</b>						
<b>1. REPORT DATE (DD-MM-YYYY)</b>		<b>2. REPORT TYPE</b>			<b>3. DATES COVERED (From - To)</b>	
<b>4. TITLE AND SUBTITLE</b>				<b>5a. CONTRACT NUMBER</b>		
				<b>5b. GRANT NUMBER</b>		
				<b>5c. PROGRAM ELEMENT NUMBER</b>		
<b>6. AUTHOR(S)</b>				<b>5d. PROJECT NUMBER</b>		
				<b>5e. TASK NUMBER</b>		
				<b>5f. WORK UNIT NUMBER</b>		
<b>7. PERFORMING ORGANIZATION NAME(S) AND ADDRESS(ES)</b>					<b>8. PERFORMING ORGANIZATION REPORT NUMBER</b>	
<b>9. SPONSORING/MONITORING AGENCY NAME(S) AND ADDRESS(ES)</b>					<b>10. SPONSOR/MONITOR'S ACRONYM(S)</b>	
					<b>11. SPONSOR/MONITOR'S REPORT NUMBER(S)</b>	
<b>12. DISTRIBUTION/AVAILABILITY STATEMENT</b>						
<b>13. SUPPLEMENTARY NOTES</b>						
<b>14. ABSTRACT</b>						
<b>15. SUBJECT TERMS</b>						
<b>16. SECURITY CLASSIFICATION OF:</b>			<b>17. LIMITATION OF ABSTRACT</b>	<b>18. NUMBER OF PAGES</b>	<b>19a. NAME OF RESPONSIBLE PERSON</b>	
<b>a. REPORT</b>	<b>b. ABSTRACT</b>	<b>c. THIS PAGE</b>			<b>19b. TELEPHONE NUMBER (Include area code)</b>	

## INSTRUCTIONS FOR COMPLETING SF 298

**1. REPORT DATE.** Full publication date, including day, month, if available. Must cite at least the year and be Year 2000 compliant, e.g. 30-06-1998; xx-06-1998; xx-xx-1998.

**2. REPORT TYPE.** State the type of report, such as final, technical, interim, memorandum, master's thesis, progress, quarterly, research, special, group study, etc.

**3. DATES COVERED.** Indicate the time during which the work was performed and the report was written, e.g., Jun 1997 - Jun 1998; 1-10 Jun 1996; May - Nov 1998; Nov 1998.

**4. TITLE.** Enter title and subtitle with volume number and part number, if applicable. On classified documents, enter the title classification in parentheses.

**5a. CONTRACT NUMBER.** Enter all contract numbers as they appear in the report, e.g. F33615-86-C-5169.

**5b. GRANT NUMBER.** Enter all grant numbers as they appear in the report, e.g. AFOSR-82-1234.

**5c. PROGRAM ELEMENT NUMBER.** Enter all program element numbers as they appear in the report, e.g. 61101A.

**5d. PROJECT NUMBER.** Enter all project numbers as they appear in the report, e.g. 1F665702D1257; ILIR.

**5e. TASK NUMBER.** Enter all task numbers as they appear in the report, e.g. 05; RF0330201; T4112.

**5f. WORK UNIT NUMBER.** Enter all work unit numbers as they appear in the report, e.g. 001; AFAPL30480105.

**6. AUTHOR(S).** Enter name(s) of person(s) responsible for writing the report, performing the research, or credited with the content of the report. The form of entry is the last name, first name, middle initial, and additional qualifiers separated by commas, e.g. Smith, Richard, J, Jr.

**7. PERFORMING ORGANIZATION NAME(S) AND ADDRESS(ES).** Self-explanatory.

**8. PERFORMING ORGANIZATION REPORT NUMBER.** Enter all unique alphanumeric report numbers assigned by the performing organization, e.g. BRL-1234; AFWL-TR-85-4017-Vol-21-PT-2.

**9. SPONSORING/MONITORING AGENCY NAME(S) AND ADDRESS(ES).** Enter the name and address of the organization(s) financially responsible for and monitoring the work.

**10. SPONSOR/MONITOR'S ACRONYM(S).** Enter, if available, e.g. BRL, ARDEC, NADC.

**11. SPONSOR/MONITOR'S REPORT NUMBER(S).** Enter report number as assigned by the sponsoring/monitoring agency, if available, e.g. BRL-TR-829; -215.

**12. DISTRIBUTION/AVAILABILITY STATEMENT.** Use agency-mandated availability statements to indicate the public availability or distribution limitations of the report. If additional limitations/ restrictions or special markings are indicated, follow agency authorization procedures, e.g. RD/FRD, PROPIN, ITAR, etc. Include copyright information.

**13. SUPPLEMENTARY NOTES.** Enter information not included elsewhere such as: prepared in cooperation with; translation of; report supersedes; old edition number, etc.

**14. ABSTRACT.** A brief (approximately 200 words) factual summary of the most significant information.

**15. SUBJECT TERMS.** Key words or phrases identifying major concepts in the report.

**16. SECURITY CLASSIFICATION.** Enter security classification in accordance with security classification regulations, e.g. U, C, S, etc. If this form contains classified information, stamp classification level on the top and bottom of this page.

**17. LIMITATION OF ABSTRACT.** This block must be completed to assign a distribution limitation to the abstract. Enter UU (Unclassified Unlimited) or SAR (Same as Report). An entry in this block is necessary if the abstract is to be limited.

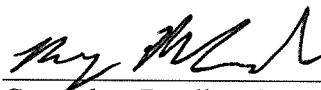
## FOREWORD

This technical report describes a constant false alarm rate (CFAR) detection algorithm along with a threshold selection algorithm derived for target detection in sonar imagery. It is designed for multi-frequency sonars and combines the advantages of template-based detection with environmental adaptation. This combination avoids the numerical estimates of a K-distribution based statistical test, while exploiting geometric features and frequency response differences between the local environment and man-made targets. The detection algorithm is based on our analysis of processed data and derived from a general statistical model. The utility of CFAR algorithms is that the selection of a detection threshold can be made independently of most image variations. However, to account for the widest variety we apply a local adaptive threshold selection mechanism and demonstrate its adaptability.

This report has been prepared, reviewed, and approved by the Science and Technology Department.



Prepared by Frank J. Crosby,  
Head, Code X20  
Unmanned Systems, Automation &  
Processing Division



Co-author Bradley C. Marchand, Code X24  
Applied Sensing and Processing Branch



Dr. Kerry W. Commander, Head, Code X  
Science & Technology Department



**CONTENTS**

**INTRODUCTION ..... 1**

**ALGORITHM OUTLINE ..... 2**

**MATCHED FILTER ..... 3**

**STATISTICAL ASSESSMENT ..... 6**

**DETECTION AND FA PROBABILITIES ..... 9**

**THRESHOLD SELECTION ..... 10**

**RESULTS..... 12**

**CONCLUSION ..... 13**

## Figures

Figure 1. Algorithm Outline .....	3
Figure 2. Matched Filter .....	4
Figure 3. Sonar data, uniform seafloor.....	5
Figure 4. Sonar data, complex seafloor .....	5
Figure 5. Smooth background matched filter output .....	5
Figure 6. Complex background matched filter output .....	6
Figure 7. Mask for mean calculation.....	8
Figure 8. F-Distribution.....	10
Figure 9. Detection values fit with exponential distribution .....	11
Figure 10. Threshold dynamics .....	12
Figure 11: FX vs. CCA .....	13

## Tables

Table 1: Desired vs. Actual False Alarm Rates .....	13
---	----



## INTRODUCTION

Detection of targets in sonar imagery presents many challenges not generally found in optical imagery. Sonars that are considered high resolution still have resolution values much coarser than most optical images. This can be seen by simple visual inspection of known object representations in the data.

When a sonar pulse is transmitted into the water, some of the sound reflects off of the target. Additionally, there are many other sources where the sound energy may reflect back towards the receiver creating interference. This scattering is caused by the many sources of inhomogeneities in the ocean. These sources may include fish, other biologics, air bubbles, dissolved elements, and particulates, as well as the ocean bottom, and surface, whereas atmospheric scattering of light is negligible in all but the most extreme cases.

Many detection algorithms for sonar imagery have been developed to address this challenging problem. Each exploits different data characteristics in an attempt to find anomalous items such as mine-like objects, unexploded ordnance, or other man-made debris. The approaches range from as general as possible to very specific.

One general approach to detection and feature extraction that has recently been explored for sonar imagery is Canonical Coordinate Analysis (CCA). The canonical coordinate decomposition method determines linear dependence or coherence between two or more data channels.<sup>1,2</sup> Canonical coordinate decomposition allows us to quantify the changes between the returns from the bottom and when target activities are present and at the same time extract useful features for target classification without the need to perform separate detection and anomaly feature extraction. This method is not based on geometry to allow target to vary greatly in shape and orientation.

At the other end of the spectrum there are model-based methods. For example, an Automatic Target Recognition (ATR) algorithm using Scale-invariant feature transform (SIFT) features.<sup>3</sup> This method physically models the 3D underwater scene. It generates simulated template images for both the target and environment. Another paper uses a similar starting point.<sup>4</sup> It also relies on a model-based approach. Each one uses a different model to reproduce three elements which are key to sonar ATR, highlight structure, seabed reverberation, and shadow zones. Both model both the targets and the backgrounds.

Several methods have also used the fusion of multiple frequency bands to improve detector performance. An adaptive clutter filter detector has been individually applied to three different sonar images varying in frequency and bandwidth.<sup>5,6</sup> Additional views of an object can be considered in a similar fashion. Rather than correlating the image data, a classification algorithm has been employed to transform the multiple-aspect classification problem into a multiple-instance learning problem.<sup>7</sup>

The method proposed in this paper is along the continuum between target agnostic and fully modeled and uses multiple frequency bands when they are available. The use of all of these sophisticated approaches is justified since the modeling of sonar data leads to inexact classical detection statistics. Initially, sonar data was widely modeled as Rayleigh distributed, since the

detected envelope of the sonar return at any given time is assumed to be the square root of the sum of the energy from many independent complex Gaussian-distributed reflectors.<sup>8</sup> However, it has been shown that in cluttered environments, the assumptions of the Rayleigh distribution approximation are inaccurate.<sup>9</sup> The number of reflectors in a local area may be reduced due to occlusion and the viewing angle of the sensor, at increasing ranges, may be highly correlated in phase due to natural textures, resulting in a probability model for pixel intensity known as the K-distribution.

The K-distribution is a compound model which consists of Gaussian speckle modulated by a slowly varying mean level, this local mean being gamma distributed. There is no closed form solution for the probability of detection in K-distributed clutter, so numerical methods are the only current method of determining a detection threshold value.<sup>10</sup>

Since closed form statistical tests are not available for pixel level decisions, we introduce a statistically valid application of the Mahalanobis distance to higher level processing. The result is an algorithm that allows for the a-priori selection of a threshold for desired performance, also known as Constant False Alarm Rate (CFAR) algorithm. The algorithm exploits the covariance between frequency bands and can be applied to any number of frequency bands, including a single band. The data presented in this paper comes from a sonar system with two such bands.

The detection algorithm and threshold selection method described in this paper has been presented for multispectral optical imagery in reference.<sup>11</sup> The multispectral application did not use the selectivity that comes with a well-defined target model. But, it did show that the detection output could vary significantly for identical targets on different backgrounds, thus necessitating an adaptive threshold method. This paper adds matched filter processing (increased selectivity) to the imagery to arrive at data which satisfies the statistical hypothesis used in the optical application.

The algorithm outline is presented in the Algorithm Outline section. The supporting reasoning is provided in the subsequent sections in the order implemented in the algorithm. The Matched Filter section describes the basis of the test statistic developed in the Statistical Assessment section. The distribution of the test statistic depends only on the number of frequency bands and the number of pixels in each sample. Since the samples may be intermixed and the distribution skewed, the test values are fit to a flexible model, which is presented in the Threshold Selection section. Fitting the actual results of the detection algorithm with a model of a portion of the theoretical output enables background-independent threshold selection. A desired false alarm rate is input into the threshold algorithm and the detections are culled accordingly. Finally, the Results section contains the results of the algorithm showing the reliability of the threshold algorithm over several background types.

## **ALGORITHM OUTLINE**

Our goal is to develop an algorithm with an automatic threshold selection mechanism. The statistical distribution of pixel values in a sonar image is generally modeled as a K-distribution. As we noted in the introduction, developing a statistical test based on this distribution is problematic. Further, such a test would be valid on a pixel level, but would ignore the additional

information inherent in the particular object recognition problem that defines our goal. There are three steps in the algorithm.

Several of these basic target characteristics, such as general size of the objects and the highlight-shadow relationship, are captured in a template or matched filter type of detector. This is the first step. Details on the matched filter application are given in the Matched Filter section.

The result of the matched filter output can then be viewed as the starting point of a more general statistical analysis. Step 2 is the statistical test based on the distribution of the matched filter correlations. From the matched filter output we evaluate target sized areas and surrounding background correlation values. Sample means and variances are calculated for these areas using convolution masks.

In an ideal case, a threshold can be chosen based on the number of frequencies and the size of the samples in the correlation analysis. We generally found consistency in form, but shifts in actual values. To accommodate these shifts, we apply a simple model to the test statistic data in step 3. This gives us a dynamic threshold that automatically updates based on data characteristics. The model and supporting reasoning is explained in the Statistical Assessment section. The chart in Figure 1 shows the algorithm outline.

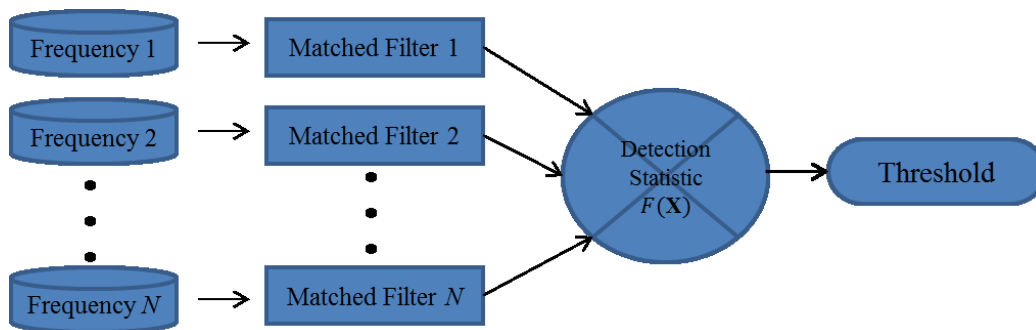


Figure 1. Algorithm Outline

## MATCHED FILTER

The basis of the matched filter detector was developed by Dobeck.<sup>12</sup> It consists of an image normalization stage followed by the matched filter step. The purpose of the normalization is to pre-condition the image so that the subsequent step is robust to variations in background level. It reduces variability due to sonar energy variation, motion compensation success, and other sonar artifacts. This is accomplished by normalizing the backgrounds throughout the image to a constant level so that highlight and shadow levels are consistent.

The normalizer uses a forward and backward filter to estimate the local background level.<sup>13</sup> The Serpentine Forward filter begins at the top of the image and selects a path along which the pixel values within the filter domain best follow the original image values. The path is generated recursively by extending the path's latest end point to one that belongs to an admissible subset of its neighbors whose intensity is most near its filtered output value. As the Serpentine Forward filter progresses, it is permitted to snake to the right or left in order to follow the best path. The

Serpentine Backward filter is defined analogous to the Serpentine Forward filter, but the image is processed from bottom to the top. The complete algorithm is presented in reference 13.

Following normalization, there are three different filters that are each applicable to specific regions in the imagery. In particular, the shadow length in the high frequency imagery increases as a function of range. This allows the filter to account for the variability of the background and mine signature as a function of range. One example of a matched filter with a short shadow is shown in Figure 2. Highlights are represented by “H” and shadow regions are represented by “S.” The exact values depend on the normalization applied. Our normalization is designed to give highlight values close to one and shadow values close to zero.

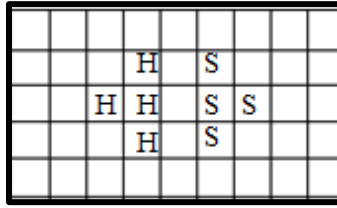


**Figure 2. Matched Filter**

Each matched filter mask contains three distinct regions: highlight, dead zone, and shadow/post-target. A different set of matched filters is used for low frequency bands. Because shadow is not a reliable phenomenon in low frequency data (due to diffraction and multi-path effects), the shadow area is significantly smaller. The matched filters,  $m(x, y)$ , are correlated with an  $N \times M$  image,  $f(x, y)$ , according to

$$I_m(i, j) = \sum_{x=0}^N \sum_{y=0}^M f(x, y) m(x - i, y - j). \quad (1)$$

The distribution of the matched filter output,  $I_m(i, j)$ , represents both positive and negative correlations. Our study found that these values tend to have a Gaussian distribution for each frequency band and across various backgrounds. These observations form the basis of the statistical tests developed in the following section.

Figure 3 and Figure 4 show some high frequency synthetic aperture sonar data that were part of the evaluation. Figure 3 shows a nearly uniform seafloor. Figure 4 is more complex, with scattered irregular structures. Figure 5 and Figure 6 show the distributions of the matched filter outputs for high and low frequencies in smooth and complex backgrounds. Figure 5 is computed from Figure 3 and Figure 6 is computed from Figure 4. The distribution results held for a variety of backgrounds and high and low frequencies. These distributions are used in the statistical tests in the next section.



**Figure 3. Sonar data, uniform seafloor**

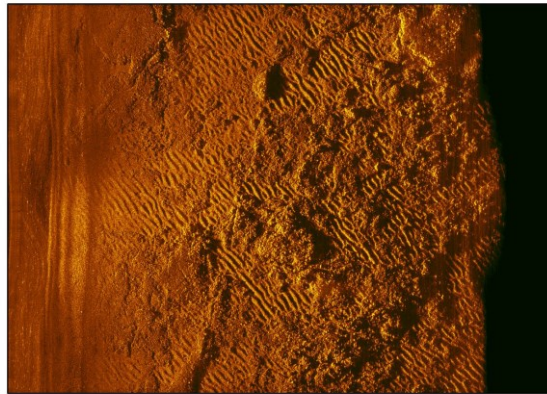


**Figure 4. Sonar data, complex seafloor**

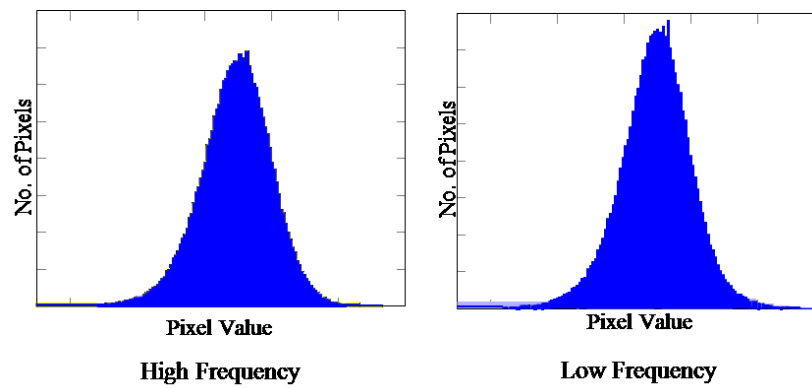


**Figure 5. Smooth background matched filter output**

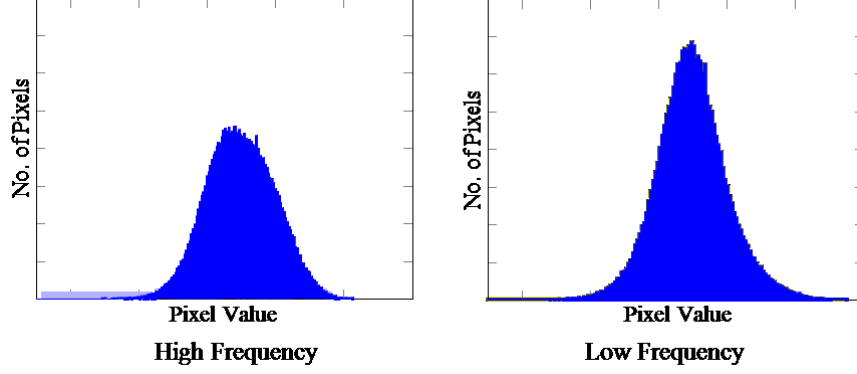


**Figure 6. Complex background matched filter output**

The statistical assessment of the following section is based on all the values; however, the values may be truncated to provide only positive correlations. It is appropriate to perform this operation at this step. Highly negative correlations are statistical anomalies, but do not likely represent desired targets.

## STATISTICAL ASSESSMENT

The K-distribution models the statistics of the backscatter from a coherent imaging process. It has successfully modelled radar backscatter from land and the sea surface and sonar images of a range of seabed sediment types. The generalized K-distribution provides a good fit to all the sediment types, including rocky, sea grass, muddy, and sandy. The K-distribution is expressed as

$$P(z) = \int_0^{\infty} P(z|x)P_c(x)dx, \quad (2)$$

where

$$P(z|x) = \frac{1}{x} \exp(-z/x) \quad (3)$$

and

$$P_c(x) = \frac{b^v x^{v-1}}{\Gamma(v)} \exp(-bx). \quad (4)$$

To determine if an area contains, as a subset, an object of interest, appropriate hypotheses are constructed. The null hypothesis is that there is no object present. If there is no object present, then the mean of the surrounding area will be similar to the mean of the possible target area. The alternative hypothesis is that there is an object present. If there is an object, then the two means will be different. The hypotheses are not based on an exact signature and therefore adapt to different conditions.

The calculation of the probability of detection in K-distributed clutter and noise is quite difficult. The probability of detection equation is given by

$$P_d(Y|x, N) = \int_Y^\infty P_R(\mu|s, N) d\mu, \quad (5)$$

where

$$P_R(\mu|s, N) = \left(\frac{\mu}{s}\right)^{(N-1)/2} e^{-(\mu+s)} \left( \sum_{i=0}^{\infty} \frac{1}{i! \Gamma(N+i)} (\sqrt{\mu s})^{N-1+2i} \right). \quad (6)$$

An approximate method that uses linear interpolation in a table has been developed.<sup>14</sup> However, the necessary tables of coefficients are only available for some models. Alternatively, the probability of detection can be calculated by numerical integration over the K-distribution in which the K-distribution is separated into its components and only the integration over the local clutter power is carried out numerically.<sup>10</sup> This represents a faster and more accurate result, but is still numerically limited.

The rest of this section defines the method to produce a test statistic which uses the matched filter selectivity and the normally distributed data that it produced. The following notation uses  $B$  and  $T$  for background and target as applied to the matched filter output, not the original sonar imagery. Given the normal distributions shown in the previous section (Figure 5 and 6) with means  $\mu_B$  and  $\mu_T$  and a common covariance,  $\Sigma$ , the hypotheses are

$$H_0: \mu_B = \mu_T \quad (7)$$

$$H_1: \mu_B \neq \mu_T. \quad (8)$$

The means are calculated by convolving the image with masks that isolate the target and use the surrounding background. The masks are shown pictorially in Figure 7. The center region is the target area. There is a guard band around the target to help avoid contamination (the white area). The guard band and the background masks are annuli around the target area. So, the three masks form concentric and non-intersecting areas. The target area has a relatively small contribution to the covariance calculation and can be omitted if the targets sought are only a few pixels. These masks allow us to calculate sample means,  $(\bar{\mu}_B, \bar{\mu}_T)$ , and a sample covariance,  $\bar{\Sigma}$ .

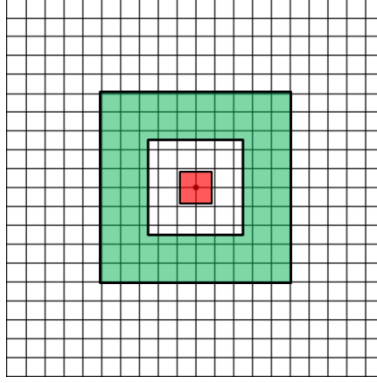


**Figure 7. Mask for mean calculation**

Broadband sonar can be divided into multiple frequency bands. Let  $p$  be the total number of bands. Then, each pixel is a  $p$ -dimensional sample that can be represented by the column vector  $\mathbf{x}_i = [x_1, x_2, \dots, x_p]^T$ , where the superscript T (non-italicized) is for transpose.

The test statistic is a scalar-valued function of the possibly multidimensional quantities: average target correlation value, the average background correlation value, and the common covariance attributable to both the background and the target.

To reliably test the hypothesis we require some knowledge of the distributions, in terms of the means and covariance. In most practical applications, the exact mean and covariance of the background and target are unknown. The assumed distributions and the samples can be used to elicit estimators for these parameters. Maximum likelihood estimators provide good estimates. Although there are several different methods for estimating unknown statistical parameters under fairly general conditions maximum likelihood estimators satisfy some desirable properties. The maximum likelihood estimator has a normal distribution with a mean equal to the true parameter with a minimum variance.

The correlation values are computed over the disjoint sets (background and target), defined by the masks in Figure 7. The total sample,  $\mathbf{X}$ , is made up of background pixels, given by  $B = [\mathbf{b}_1, \mathbf{b}_2, \dots, \mathbf{b}_{N_B}]$ , and the possible target pixels,  $T = [\mathbf{t}_0, \mathbf{t}_1, \dots, \mathbf{t}_{N_T}]$ . The number of pixels used in the detection calculation is the sum of the two samples, denoted by  $N = N_B + N_T$ . The sample vector mean of the background pixels is given by  $\sum \mathbf{b} / N_B = \bar{\mu}_B$ . Similarly, the sample target mean is  $\sum \mathbf{t} / N_T = \bar{\mu}_T$ .

The null hypothesis defines a subset of the parameter space. Let  $\omega$  be the set of points in the parameter space that correspond to  $H_0$  and let  $\Omega$  be the set of all points in the parameter space. For our example,  $\omega = \{(\mu_B, \mu_T) : \mu_B = \mu_T, -\infty < \mu_B, \mu_T < \infty\}$  and  $\Omega = \{(\mu_B, \mu_T) : -\infty < \mu_B, \mu_T < \infty\}$ . By utilizing the likelihood function we can judge if a particular sample of the background and target does not support  $H_0$ . Let the sample be given and let  $L(\hat{\omega})$  be the



likelihood function maximized with respect to parameters in  $\omega$ , and let  $L(\hat{\Omega})$  be the likelihood function maximized with respect to parameters in  $\Omega$ . The likelihood ratio is

$$\frac{L(\hat{\omega})}{L(\hat{\Omega})} = \left[ \frac{1}{1 + \left( N_B N_T / N \right)^{1/2} (\bar{\mu}_B - \bar{\mu}_T)^T \mathbf{A}^{-1} \left( N_B N_T / N \right)^{1/2} (\bar{\mu}_B - \bar{\mu}_T)^T} \right]^{N/2}, \quad (9)$$

where

$$\mathbf{A} = \sum_{i=1}^{N_B} (b_i - \bar{\mu}_B)(b_i - \bar{\mu}_B)^T + \sum_{i=1}^{N_T} (t_i - \bar{\mu}_T)(t_i - \bar{\mu}_T)^T. \quad (10)$$

The inequality  $\frac{L(\hat{\omega})}{L(\hat{\Omega})} \leq k$  is equivalent to

$$F(\mathbf{X}) = \frac{N_B N_T}{N} (\bar{\mu}_B - \bar{\mu}_T)^T \mathbf{S}^{-1} (\bar{\mu}_B - \bar{\mu}_T) \geq (k^{-2/N} - 1)(N - 2), \quad (11)$$

with  $\mathbf{S} = \mathbf{A} / (N - 2)$ .

The criterion states that the critical region for a test of  $H_0$  against  $H_1$  is defined by the set of points in the sample space for which  $L(\hat{\omega}) / L(\hat{\Omega}) \leq k$ , where  $k$  is selected so that it has the desired level of significance. The value  $F(\mathbf{X})$  is our detection statistic.

## DETECTION AND FA PROBABILITIES

Recalling that the distributions of the background and target pixels were normally distributed,  $N(\mu_B, \Sigma)$  and  $N(\mu_T, \Sigma)$ , the sample means of the background,  $\bar{\mu}_B$ , and target,  $\bar{\mu}_T$ , are distributed according to  $N(\mu_B, 1/N_B \Sigma)$  and  $N(\mu_T, 1/N_T \Sigma)$ , respectively. Additionally,

$$\delta = \left( N_B N_T / N \right)^{1/2} (\mu_B - \mu_T) \quad (12)$$

is normally distributed with zero mean and covariance  $\Sigma$ .

The term  $\mathbf{S}$  was derived from

$$\mathbf{A} = \sum_{i=1}^{N_B} (b_i - \bar{\mu}_B)(b_i - \bar{\mu}_B)^T + \sum_{i=1}^{N_T} (t_i - \bar{\mu}_T)(t_i - \bar{\mu}_T)^T. \quad (13)$$

Because  $\mathbf{A}$  can be written as  $\sum_i \mathbf{Z}_i \mathbf{Z}_i^T$ , where each  $\mathbf{Z}_i$  is independent with distribution  $N(0, \Sigma)$  so can  $(N - 2)\mathbf{S}$ . Under these conditions, it can be shown that  $F(\mathbf{X})$  is distributed as a noncentral  $F$

with  $p$  and  $N-p-1$  degrees of freedom and  $\delta$  as the noncentrality parameter.<sup>15</sup> A graph of the F-distribution is shown in Figure 8.

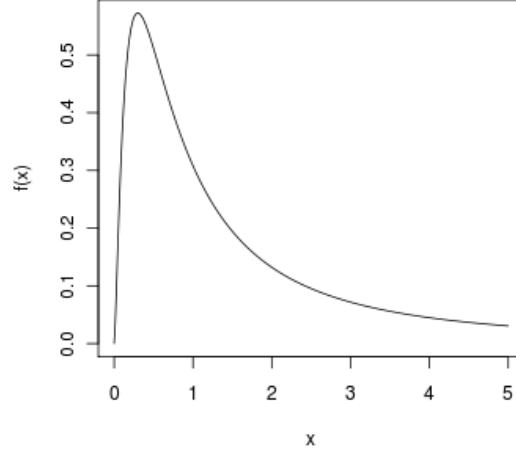


**Figure 8. F-Distribution**

Since the noncentrality parameter is nonzero under  $H_1$ , computation of the probability of detection requires knowledge of the target and background distributions. The probability of detection is equal to the probability of rejecting  $H_0$ , when  $H_1$ , is true. This is calculated as

$$\begin{aligned} P_d &= P \left\{ \left[ \frac{N-p-1}{p(N-2)} \right] \frac{N_B N_T}{N} (\mu_B - \mu_T)^T S^{-1} (\mu_B - \mu_T) \right. \\ &\quad \left. \geq \left[ \frac{N-p-1}{p(N-2)} \right] (k^{-2/N} - 1)(N-2) | H_1 \text{ true} \right\} \\ &= 1 - F_{\delta, p, N-p-1} \left\{ \left( \frac{N-p-1}{p(N-2)} \right) k^{-2/N} - 1 \right\}. \end{aligned} \quad (14)$$

The number  $k$  is the threshold for the detection metric and  $F_{\delta, p, N-p-1}$  denotes a noncentral F-distribution with  $\delta$  as the noncentrality parameter and  $p$  and  $N-p-1$  degrees of freedom.

The probability of a false alarm  $P_{fa}$  is equal to the probability of rejecting  $H_0$  when  $H_0$  is true. The noncentrality parameter becomes zero under  $H_0$ . The value  $P_{fa}$  is given by

$$\begin{aligned} P_{fa} &= P \left[ \frac{N_B N_T}{N} (\mu_B - \mu_T)^T S^{-1} (\mu_B - \mu_T) > (k^{-2/N} - 1)(N-2) | H_0 \text{ true} \right] \\ &= 1 - F_{0, p, N-p-1} \left[ \left( \frac{N-p-1}{p} \right) (k^{-2/N} - 1) \right] \end{aligned} \quad (15)$$

where  $F_{0, p, N-p-1}$  denotes a central F-distribution with  $p$  and  $N-p-1$  degrees of freedom.

## THRESHOLD SELECTION

Ideally the threshold is selected based on the F-distribution using the number of pixels in the samples,  $N$ , and the number of sonar bands,  $p$ . However, the probability of detection requires

specific knowledge of the true means of the correlation values and there may be shifts in the correlation values that also have an effect on the probability of false alarm. Additionally, the lower values of the F-distribution are affected by loss of significant figures that stems from the subtractions in the  $F(\mathbf{X})$  calculation. Both of these shortcomings are overcome by an approximation to the significant portion of the F-distribution as determined by the observed final values.

The F-distribution, after its peak value, can be approximated with the exponential distribution. The peak can easily be identified on a local basis, image by image or other suitable partition.

The probability density function corresponding to the exponential distribution is  $g(x) = (1/\mu)\exp(-x/\mu)$ .

Whereas the F-distribution had  $p$  and  $N$  as parameters, the exponential distribution has  $\mu$ , the distribution mean, as a single parameter. The mean is estimated from the final values above the F-distribution peak value. Further, this estimation enables the distribution to shift independently from image to image based on the observed data. The derivation of the F-distribution assumed that the correlation values followed the Gaussian distribution. Using the modeled exponential distribution, we are better able to handle deviations.

Figure 9 is a histogram of detection values fit with an exponential density function. Histograms are computed and fit for each image. The fit is rather poor for the first few bins, but is fairly accurate in the last few. In cases where only a few false alarms are desired, it is the last few that are responsible for agreement between the desired number of false alarms and the number produced by the threshold selection method.

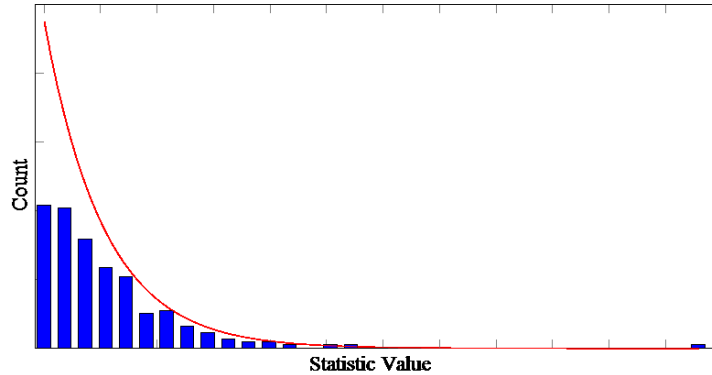


**Figure 9. Detection values fit with exponential distribution**

The mean is estimated using the detection values as discrete samples of the continuous exponential distribution. The desired number of false alarms per image is calculated using the distribution function,  $G$ , and the number of samples,  $N$ . The distribution function is given by

$$G(x) = \begin{cases} 0, & -\infty < x < 0 \\ 1 - \exp(-x/\mu), & 0 \leq x < \infty. \end{cases} \quad (16)$$

If  $K$  is the desired number of elements that are expected to be greater than a threshold  $T$ , then the equation is  $[1 - G(T)]N < K$ . Solving for  $T$  gives:

$$1 - [1 - \exp(T/\mu)] < \frac{K}{N} \quad (17)$$

$$T \geq -\mu \ln(K/N). \quad (18)$$

Using equality in the final equation for  $T$  assures that the threshold is calculated to be the lowest possible to achieve the desired number of false alarms. A consequence of selecting the lowest threshold is that it is not uncommon that  $K$  false alarms are encountered.

## RESULTS

A range of desired false alarm values were selected for testing. The test set consisted of 351 dual frequency synthetic aperture sonar images made up of both uniform and uneven backgrounds. The wide variety of backgrounds was necessary to show adaptability of the threshold selection method. The threshold is dynamically selected for each image based on the overall selected number of desired false alarms. Figure 10 is a histogram of the threshold values. The thresholds are concentrated in the teens, but vary over a significant range as the method adapts to differing backgrounds.

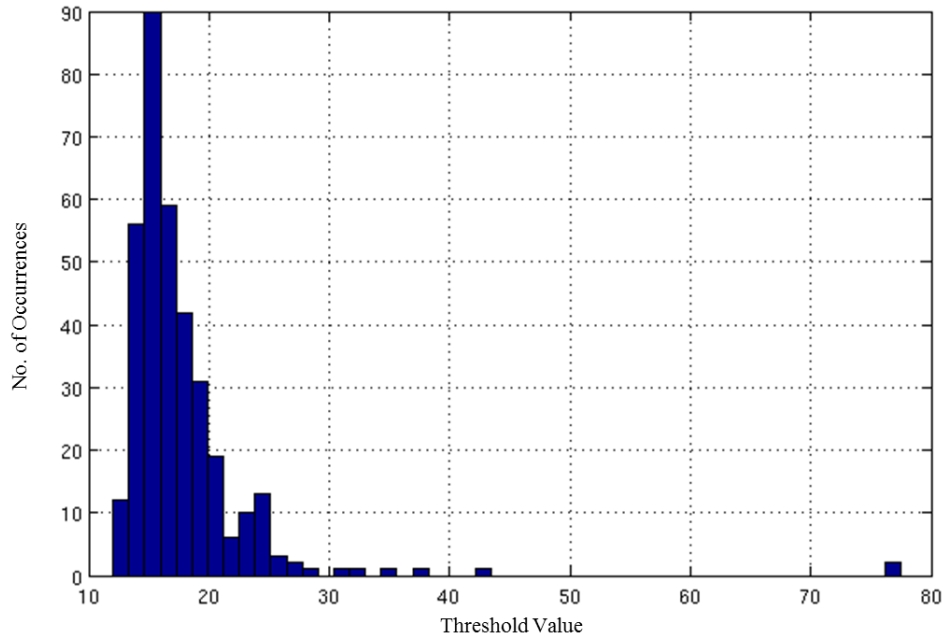


**Figure 10. Threshold dynamics**

The selected values and the actual false alarm rates (FAR) are given in Table 1. The FAR shown is average false alarms per image. There is a noteworthy discrepancy between the  $K$ -value and the actual number of false alarms. However, the relationship is nearly linear across the tested

values. Thus, it is possible to predict performance and choose a  $k$ -value based on the sought after number of false alarms, which is the desired property.

**Table 1. Desired vs. Actual False Alarm Rates**

K values	5.0	2.0	1.0	0.5	0.25	0.1	0.01
Actual FAR	32.99	10.45	4.98	2.81	1.89	1.36	0.88

We also compared this detection method with the CCA method.<sup>1</sup> This FX based method calculates a dynamic threshold and so a traditional Receiver Operating Characteristic (ROC) curve is not directly applicable. While it is possible to produce a ROC-like curve for the  $F(\mathbf{X})$  method using various  $k$  values, the actual threshold applied to the data is not constant for any particular value. The graph of the two methods is shown in Figure 11. The vertical axis represents the percentage of mine-like targets found in the data. The solid curve is the ROC for the CCA method. The circles are the performance of the  $F(\mathbf{X})$  method for distinct  $k$  values (as indicated by the adjacent text).

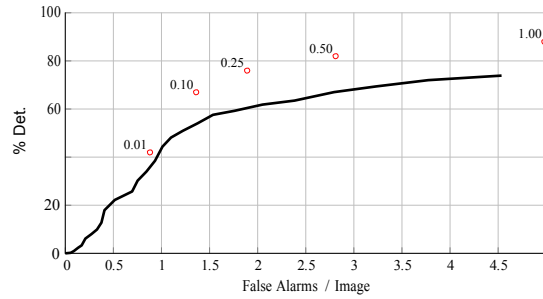


**Figure 11: FX vs. CCA**

Detection is typically followed by feature extraction and classification in automatic target recognition.<sup>16,17</sup> Classification methods can be computationally intensive and so the function of the detection stage is to eliminate most of the data, so that the more intensive algorithmic elements are not overburdened. The competing requirement is that targets of interest are not filtered out. The graph in Figure 11 shows that for a fixed number of false alarms, the FX method passes more detections than the CCA method, particularly in the one-to-three false alarms per image values.

## CONCLUSION

This work presents a constant false alarm rate (CFAR) detection and threshold selection algorithm for sonar imagery. It uses a multi-frequency matched filter element for selectivity and is based on the statistical properties of that output. These properties allow for the use of an automated threshold selection procedure. Rather than trying to experimentally adjust a threshold to achieve a desired output, a user can select the desired output and allow the procedure to dynamically set the threshold. The desired output is determined by a clear and obvious process. This entire algorithm is designed to avoid the numerical estimates of a K-distribution based statistical test, while exploiting geometric features and frequency response differences between the local environment and man-made targets.

## References

1. Azimi-Sadjadi, M. R., and Tucker, J. D., "Target detection from dual disparate sonar platforms using canonical correlations," in *Proceedings SPIE—Int. Soc. Opt. Eng.*, Vol. 6953, Mar 2008, DOI: 10.1117/12.776465.
2. Tucker, J.; Derek, Azimi-Sadjadi, M. R., "Coherence-based Underwater Target Detection from Multiple Disparate Sonar Platforms," *IEEE Journal of Oceanic Engineering*, Vol. 36, No. 1, 2010.
3. Zhu, Zhaotong; Xu, Xiaomei; Yang, Liangliang; Yan, Huicheng; Peng, Shibao; Xu, Jia, "A model-based Sonar image ATR method based on SIFT features," *OCEANS 2014 - TAIPEI*.
4. Groen, J.; Coiras, E.; Del Rio, J.; Evans, Vera B., "Model-based sea mine classification with synthetic aperture sonar," *Radar, Sonar & Navigation, IET*, Vol. 4, Issue: 1, 2010, pp. 62-73.
5. Aridgides, T., and Fernandez, M.F., "Automated target classification in high resolution dual frequency sonar imagery," in *Proceedings SPIE, Int. Soc. Opt. Eng.*, Vol. 6553, Apr 2007, DOI: 10.1117/12.717739.
6. Aridgides, T., and Fernandez, M., "Enhanced ATR algorithm for high resolution multi-band sonar imagery," in *Proceedings SPIE, Int. Soc. Opt. Eng.*, Vol. 6953, Mar 2008, DOI: 10.1117/12.773304.
7. Wang, Xiaoguang; Liu, Xuan; Japkowicz, N.; Matwin, S.; Nguyen, Bao, "Automatic Target Recognition using multiple-aspect sonar images," in *Evolutionary Computation (CEC), 2014 IEEE Congress on*, 2014, pp. 2330-2337, DOI: 10.1109/CEC.2014.6900261.
8. Burdick, W., *Underwater Acoustic System Analysis*, Second Edition, Prentice Hall, Englewood Cliffs, NJ, 1991.
9. Dunlop, J., "Statistical modelling of sidescan sonar images," *IEEE/MTS OCEANS*, Vol. 1, 1997, pp. 33-38.
10. Bocquet, Stephen, *Calculation of Radar Probability of Detection in K-Distributed Sea Clutter and Noise*, Joint Operations Division DSTO Defence Science and Technology Organisation, AR 014-977, April 2011, Canberra ACT 2600, Australia.
11. Crosby, F., "Signature adaptive target detection and threshold selection for constant false alarm rate," *Journal of Electronic Imaging*, Vol. 14, No. 3, 2005.
12. Dobeck, G.; Hyland, J.; Smedley, L., "Automated Detection/Classification of Sea Mines in Sonar Imagery," in *Proceedings SPIE*, Vol. 3079, 1997.

- 13 Dobeck, G., "Image Normalization using the Serpentine Forward-Backward Filter: Application to high-resolution sonar imagery and its impact on mine detection and classification," in *Proceedings SPIE*, Vol. 5794, 2005, DOI: 10.1117/12.602878.
- 14 Watts, S., "A practical approach to the prediction and assessment of radar performance in sea clutter," in *IEEE International Radar Conference*, 1995.
- 15 Morrison, D. F., *Multivariate Statistical Methods*, Duxbury Press, 2005.
- 16 Fei, T.; Kraus, D.; Zoubir, A. M., "Contributions to Automatic Target Recognition Systems for Underwater Mine Classification," in *IEEE Geoscience and Remote Sensing*, IEEE Transactions on Year: 2015, Vol. 53, Issue: 1, 2015, pp. 505-518, DOI: 10.1109/TGRS.2014.2324971.
- 17 Kriminger, E.; Cobb, J. T.; Principe, J.C., "Online Active Learning for Automatic Target Recognition," *Oceanic Engineering*, IEEE Journal of Year: 2014, Vol. PP, Issue: 99, pp. 1-9, DOI: 10.1109/JOE.2014.2340353.

## DISTRIBUTION

Defense Technical Information Center ATTN DTIC-0 8725 John J. Kingman Road Fort Belvoir, VA 22060-6218	1
Naval Surface Warfare Center, Panama City Division ATTN: Technical Library Code 1033 110 Vernon Avenue Panama City, FL 32407-7001	2
Naval Surface Warfare Center, Panama City Division ATTN: Code X20, Dr. Frank Crosby 110 Vernon Avenue Panama City, FL 32407-7001	1
Naval Surface Warfare Center, Panama City Division ATTN: Code X24, Mr. Bradley C. Marchand 110 Vernon Avenue Panama City, FL 32407-7001	1



